JOURNAL OF MATERIALS SCIENCE 33 (1998) 833–837

Hardening and phase stability in rapidly solidified Al–Fe–Ce alloys

M. FASS, D. ELIEZER, E. AGHION
Ben-Gurion University of the Negev, Beer Sheva, Israel
F. H. FROES
University of Idaho, Moscow, ID, USA

Rapidly solidified (RS) Al–Fe–Ce alloys were prepared by melt spinning. The phases present and the thermal stability, at temperatures up to 500 °C, were then followed by X-ray analysis, chemistry, hardness and thermal analysis techniques. The results obtained indicated that the alloys studied have enhanced mechanical properties compared to commercial aluminium alloys and castings of the same alloy compositions, and the RS alloy also exhibit good stability up to about 300 °C; a result of stable second phase particles. It is suggested that these results indicate that there are two mechanisms responsible for the hardening and stability of the RS alloys: solid solution strengthening at lower temperatures, and semicoherent particles formed from supersaturated solid solution at higher temperature. The maximum hardness, after 2 h ageing occurred at about 300 °C. At higher temperatures the dispersed phase became incoherent with a dramatic loss in hardness. © *1998 Chapman & Hall*

1. Introduction

Rapidly solidified (RS) alloys with addition(s) of transition metals and rare earths, such as iron, nickel, cobalt, cerium, erbium, neodymium, gadolinium [1–10], offer excellent potential elevated temperature applications. In particular, these alloys are characterized by enhanced high temperature tensile strength with usable ductility, good thermal stability and attractive creep properties up to and above 300 °C.

There are little reported data on binary Al–rare earth (RE) alloys produced by RS. The Al–Ce system has been investigated by Yakunin and Ryabtsev [11]. They found that the solid solubility of Ce in Al was increased to about 1.9% by RS at a cooling rate of about 10^6 °C s^{-1}.

Although much work has been reported on the binary Al–Fe system [13, 14] and on conventional ternary additions such as V [15] or Zr [16], including their thermal stability, there are little reported data on Al–Fe alloys containing rate earth metals.

The majority of the work carried out to date on this type of system was conducted on Al–Fe–MM (MM misch metal; assumed to have the composition 27 at %La, 48 at %Ce, 5 at %Pr, 16 at %Nd and other 4 at % rare earths which are assumed to behave as 2 at %Gd and 2 at %Y) [17, 18].

The purpose of the present study is to provide a more complete description of the structure, hardening mechanism and the heat treatment response of one specific RS Al–Fe–Re alloys, Al–Fe–Ce.

2. Experimental procedure

2.1. Material production

Small (100 g) ingots of binary Al–10.3 wt% Ce and Al–8 wt% Fe and ternary Al–8 wt% Fe–4 wt% Ce alloys, were produced using non-consumable arc melting of elemental constituents on a water cooled copper hearth. Ribbons were prepared from each alloy by melt spinning onto a cooled copper wheel [19]. The melt temperature as measured by a disappearing filament pyrometer was 1300 °C. The copper wheel was 0.3 m diameter, rotating at 1400 r.p.m., giving a peripheral velocity of 20.4 m s^{-1}. Prior to each run, the periphery of the wheel was cleaned with 600 grit silicon carbide paper and washed with acetone. The average thickness of the melt spun ribbon was about 60 μm and the ribbons were 2–3 mm wide.

2.2. Heat treatment

The ribbons were isochronally annealed in vacuum for 2 h at temperatures ranging from 100 to 500 °C.

2.3. Microhardness

Microhardness measurements were made using an automatic machine (Ternary automatic micro hardness system) with a Knoop indenter with a load at 10 g and a dwell time of 15 s. A minimum of 30 indentations were made on lightly etched samples.

2.4. Microstructural evaluation

The microstructures of the ribbons were studied optically and using scanning electron microscope (SEM) Five pieces of each lot, i.e. alloy and annealing treatment, were used for optical examination. These samples were cleaned in an ultrasonic bath with acetone and mounted in epoxy resin. Standard polishing techniques were then used to prepare sections for optical microscopy and microhardness measurements. For optical metallography the samples were etched using 50% Keller's reagent in water at room temperature.

SEM examination was carried out on the metallographic section using normal imaging techniques and chemical analysis.

Specimens for transition electron microscopy (TEM) were prepared from the ribbons by cutting the ribbons in three very thin areas near holes present in the as-cast RS ribbon. The microstructure in these regions was found to be "A" structure [20]. The TEM was operated at 80 keV.

Using an amorphous adhesive spray, short pieces (15 mm) of ribbons were glued to a glass slide and X-ray diffractometry (XRD) performed. An equal exposed area was used for all samples.

2.5. Differential scanning calorimetry (DSC) analysis

DSC measurements were performed using a Perkin–Elmer thermal analysis system in high purity argon. Samples from room temperature were heated up to 600 °C at the rate of 20 °C min^{-1}. The sample was then cooled down slowly (within 10 min) and held at 25 °C for another 10 min. Reheating was then carried out at a rate of 20 °C min^{-1}, again to 600 °C. The sample current heat flow was measured in the two runs as a function of temperature. A second series of experiments was then conducted on the Al–10.3 wt% Ce alloy only. In these experiments an alloy sample was maintained at fixed temperatures of 300, 400 and 500 °C. All samples were maintained until the sample current heat flow was constant and the time required for the sample current heat flow to stabilize was recorded.

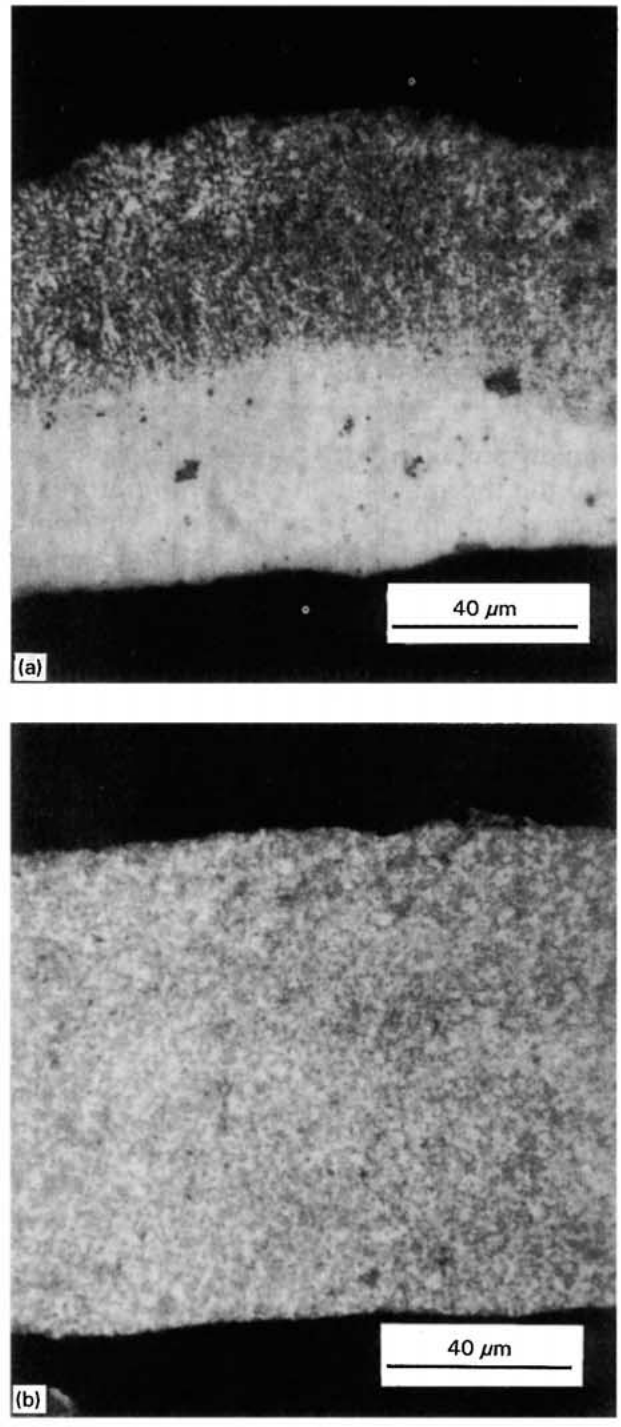

Figure 1 (a) Al–8 wt%Fe–4 wt%Ce as-cast melt spun ribbon longitudinal section, and (b) after 2 h heat treatment at 500 °C.

3. Results and discussion

The optical microstructure of longitudinally cross-sectioned ribbons of the Al–8 wt% Fe–4 wt% Ce alloy in the as-cast melt spun condition shows a featureless, zone A [20], region next to the wheel contact surface (Fig. 1a). This zone is quite narrow, about 20 μm in width, and typical of most of the alloys investigated this work. Next to this zone A is a region showing a refined dendritic structure extending to about 10% of the ribbon thickness. The rest of the thickness consists of a (zone B [20]) cellular structure. Fig. 1b shows the same sample after heat treatment at 500 °C for 2 h. A fine uniform microstructure is present, however, in the as-cast zone A.

Knoop microhardness measurements were made on five samples from each lot taken from different parts of the ribbon. In all cases two indentations were made on the longitudinal cross-section plane and three in the transverse cross-section plane.

Samples of approximately the same thickness (50–70 μm) were selected to eliminate the possible effect of variations in cooling rate. Measurements were taken randomly along the centreline of zones A and B. The long axis of the indentation was made parallel to the long dimension of the sample. Fig. 2a,b shows the result of microhardness measurements as a function of heat treatment temperature for the Al–10.3 wt%Ce and

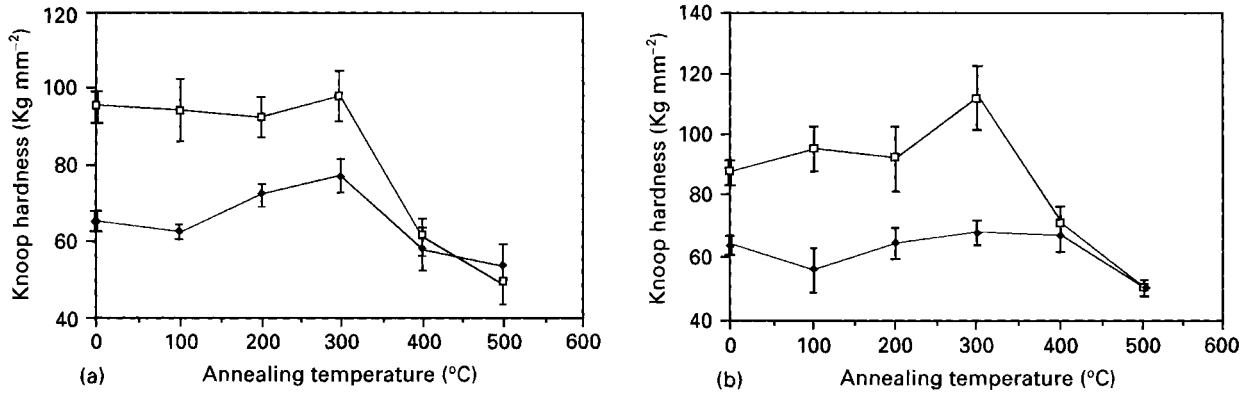

Figure 2 Knoop microhardness results as a function of 2 h heat treatment temperature for (a) Al–10.3 wt%Ce, and (b) Al–8 wt% Fe–4 wt%Ce ribbons: (□) wheel side, (◆) air side.

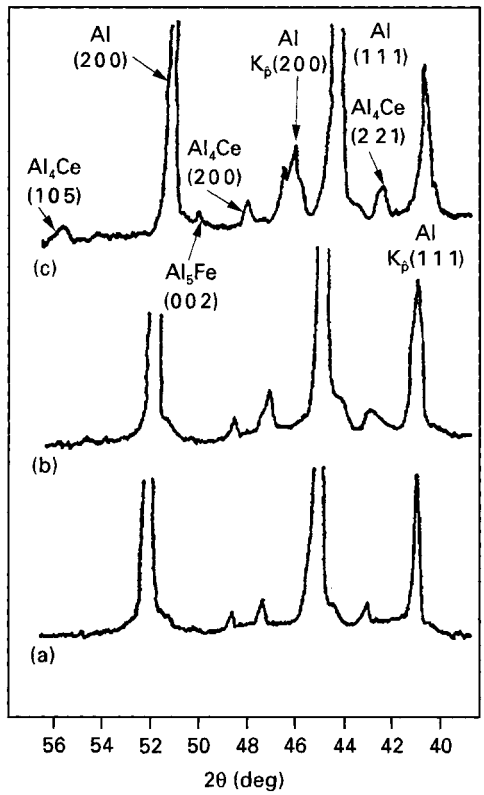

Figure 3 X-ray diffraction from Al–8 wt%Fe–4 wt%Ce at (a) room temperature, (b) 300 °C, and (c) 500 °C.

Al–8 wt% Fe–4 wt%Ce alloys in both zones A and B. These results are typical of other samples characterized in this study.

Microhardness results show clearly that all the alloys maintained their hardness up to a temperature of more than 300 °C. At about 400 °C, the hardness dropped to annealed Al levels. All the alloys displayed an ageing phenomenon with peak hardness at about 300 °C (for the 2 h anneal used). The ternary alloys show higher hardness than the binary alloys, especially after heat treatment at 300 °C.

X-ray diffraction results obtained from RS and conventionally cast Al–Fe–Ce are shown in Fig. 3. These results indicate a shift in the aluminium and intermetallic peaks position. Fig. 4 represents the change in the peak width and position caused by the RS process and by heat treatment. In both figures heat treatment at temperatures over 300 °C returns the peak position and width to the conventionally cast configuration.

The change in the peak position indicates that the lattice parameter increased as a result of the RS process. These results indicate that RS ribbons exhibit internal stresses typical of solid solution hardened alloys.

The results of the DSC tests are shown in Figs 5–7. In Fig. 5 a primary DSC curve from the as-cast RS Al–8 wt%Fe ribbon is shown from room temperature to about 550 °C, and compared to a secondary heating cycle for the same sample. A major reaction occurs at approximately 400 °C. It has been pointed out [19, 20] that the maximum reaction rate corresponds to the peak of the DSC curve. Fig. 6 presents the same curve for Al–20.3 wt%Ce. The major reaction here occurs at approximately 350 °C. A similar behaviour was found [21] for Al–Li and Al–Be–Li alloys. DSC curves for annealing at fixed temperatures of 500, 400 and 300 °C for Al–10.3 wt%Ce are shown in Fig. 7a,b. The stabilization time at 500 °C is 75 min and at 400 °C it is 150 min, while more than 450 min are required for stabilization at 300 °C.

Energy dispersive spectroscopy (EDX) analysis in the SEM indicated that chemistry was uniform through the ribbon section despite the changes in microstructure. Fig. 8 shows a line scan on Er concentration carried out on the Al–10.3 wt%Ce ribbon section. This result indicates that most of the alloying element is in solid solution.

Analysis of the XRD pattern identified the structure as an aluminium. The secondary phases were identified as Al–3 wt%Fe and Al_4Ce. These phases are generally coherent with the α-aluminium matrix with a {2 1 1} habit phase.

The average size of the second phase as a function of heat treatment temperature was determined. The size distribution is very non-uniform, which causes a relatively large scatter in the sizes determined. At a hardness of approximately 110 H_V and the $1/d_m$ values. These results are also consistent with the Orowan model of dislocations bypassing non-shearable precipitates.

The linear relation obtained can be written as

$$H_V = K_1/d_s + K_2$$

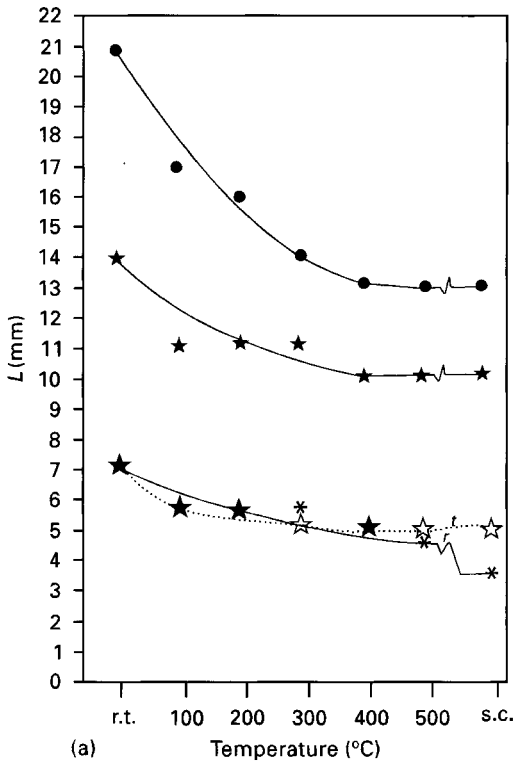

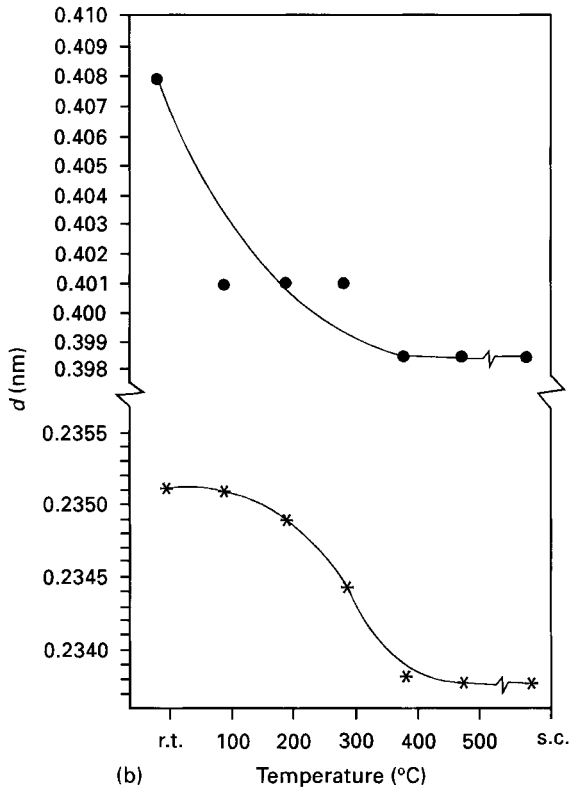

Figure 4 Change in peaks (a) width, L, and (b) position, d: (●) Al (1 1 1) base, (☆) Al (1 1 1) half peak height, (★) Al_4Ce (1 0 1) base, (*) Al_4Ce (1 0 1) half peak height.

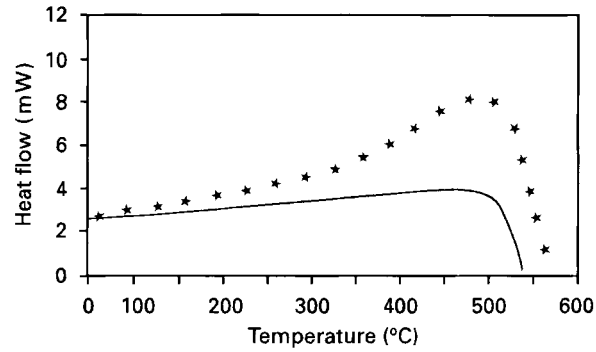

Figure 5 Results of DSC test in Al–8 wt%Fe.

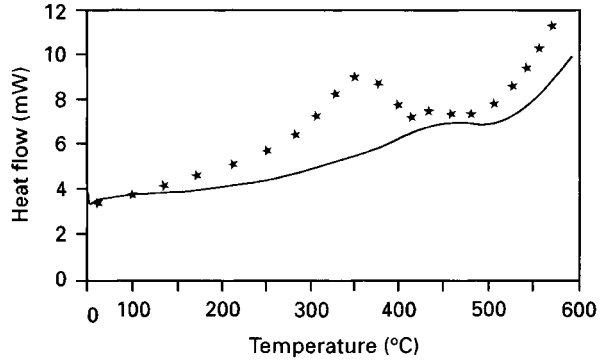

Figure 6 Results of DSC test in Al–20.3 wt%Ce

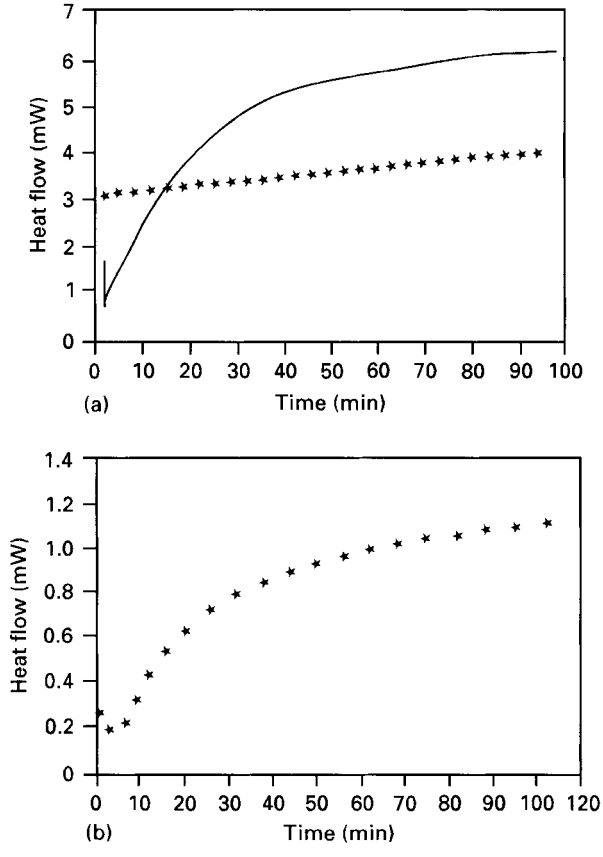

Figure 7 Fixed temperature DSC results for Al–10.3 wt%Ce at (a) 500 °C, and (b) 400 °C.

where H_V is Vickers hardness number and d_s is in μm; the constants K_1 and K_2 are 1.6 and 55 (1.567 and 89.77 by Dermarker [22]), respectively. Despite the larger scatter, the data indicated that the particles coarsen significantly at temperatures about 300 °C. Below 300 °C little coarsening is observed. This observation of particle coarsening is consistent with the DSC and hardness results.

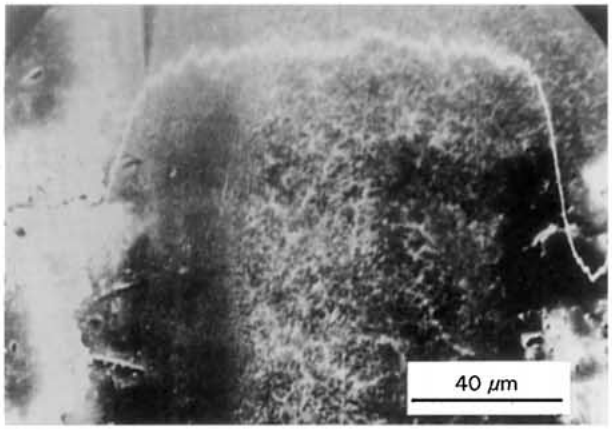

Figure 8 Profile of the element Ce using the EDX technique for as-received Al–10.3 wt%Ce.

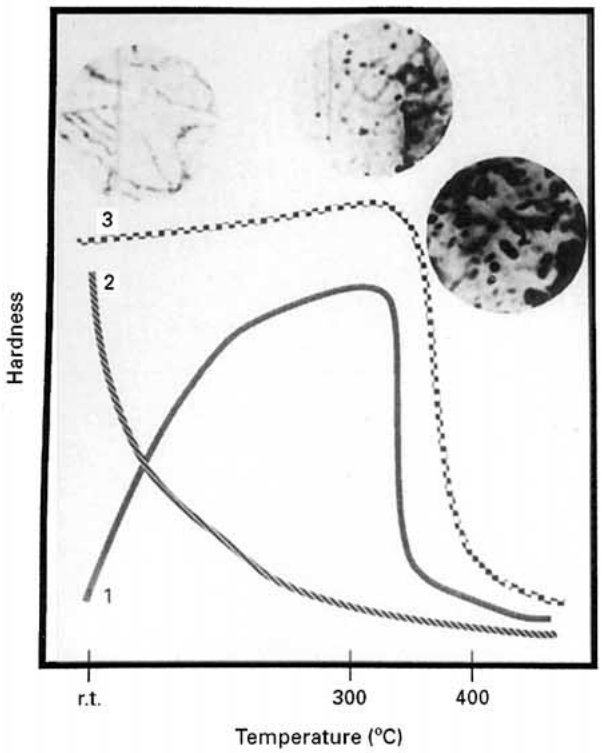

Figure 9 The total hardness (-·-·-) from solid solution (////) and precipitation (—).

The results obtained in this investigation indicate that there are two mechanisms responsible for the hardening of the RS Al–RE alloys. The first mechanism is hardening by solid solution which occurs because of initiation and growing of stable semicoherent secondary phases particles from the supersaturated solid solution at higher temperature. The maximum hardening from these two mechanism was obtained at about 300 °C (for 2 h hold). At higher temperatures the second phase particles become incoherent and at about 500 °C the hardness drops to that of annealed aluminium. A summary of the resulting hardening mechanisms proposed is shown in Fig. 9.

4. Conclusions

The phases occurring and the hardening which takes place in rapidly solidified Al–8 wt%Fe, Al–20.3 wt%Ce and Al–8 wt%Fe–4 wt%Ce ribbons have been characterized. The conclusions from this study are as follows.

1. Two mechanisms contribute to the hardening of these materials. The first mechanism is hardening by solid solution which occurs at low temperatures. The second contribution comes from a dispersion hardening effect which acts as a result of initiation and growth of stable semicoherent secondary phase particles.

2. Microhardness in zone A type microstructure averages about 100 H_V and about 60 H_V in zone B type microstructure.

3. The general ageing characteristics of Al–Fe–RE alloys studied are very similar.

4. Heat treatment coarsens the microstructure, probably by diffusion controlled processes.

5. The size distribution of the second phase particles is not uniform. Upon heat treatment at temperatures greater than 300 °C these particles coarsen and the growth behaviour of these particles follows a diffusion controlled growth mechanism.

References

1. M. FASS, D. ITZHAK, F. H. FROES and D. ELIEZER, *J. Mater. Sci. Lett.* **61** (1987) 227.
2. *Idem, ibid.* **7** (1988) 76.
3. W. M. GRIFFITH, R. E. SANDERS and G. J. HILDEMAN, "High Strength Powder Metallurgy Aluminum Alloys" edited by M. Koczak and G. J. Hildeman (TMS Warrendale, PA, 1982). p. 209.
4. G. THURSFIELD and M. J. STOWELL, *J. Mater. Sci.* **9** (1974) 1644.
5. C. M. ADAM, in "Rapidly Solidified Amorphous and Crystalline Alloys", edited by B. H. Kear, B. C. Giessen and M. Cohen (Elsevier, New York, 1982).
6. M. E. FINE and J. R. WEERTMAN, "Synthesis and Properties of Elevated Temperture P/M Aluminum Alloys", Annual Report, AFOSR-82-005, (Air Force Office of Scientific Research, 1984).
7. Y. W. KIM and W. M. GRIFFITH, "Rapidly Solidified Powder of Aluminum Alloys", edited by M. E. Fine and E. A. Starke Jr, ASTM STP 890 (American Society for Testing and Materials, Philadelphia, PA, 1986). p. 485.
8. Y. W. KIM and A. G. JACKSON, *Scripta Metall.* **20** (1986) 777.
9. L. BENDERSKY, *Met. Trans* **16A** (1985) 683.
10. S. J. SAVAGE, D. ELIEZER and F. H. FROES, *ibid.* **18A** (1987) 1533.
11. A. A. YAKUNIN and S. I. RYABTSEV, "Problems Relating to Metastable Cast Alloy Structures" (Drepropetrovsk State University, 1981) p. 28.
12. C. WILKINSON, *Acta Crystallog.* **22** (1967) 924.
13. S. J. SAVAGE and F. H. FROES, *J. Metals* **36**(4) (1984) 20.
14. H. JONES, *Mater. Sci. Engng* **65** (1984) 145.
15. Y. WASEDA and K. T. AUST, *J. Mater. Sci.* **16** (1981) 2337.
16. S. SRIRAM and J. A. SEKHAR, *Mater. Sci. Engng* **66**(1) (1984) L9.
17. A. K. GOGIA, P. V. RAO and J. A. SEKHAR, *J. Mater. Sci.* **20** (1985) 3091.
18. H. JONES, *Mater. Sci. Engng* **5** (1969) 1.
19. H. E. KISSINGER, *Anal. Chem.* **29** (1957) 1702.
20. E. LOUIS and C. GARCIA-CORDOBILLA, *J. Mater. Sci. Lett.* **19** (1984) 689.
21. T. G. NIEH, A. R. PELTON, W. C. OLIVER and J. WADSWORTH, *Met. Trans.* **19A** (1988) 1173.
22. S. DERMARKER, in "Rapidly Solidified Powder of Aluminum Alloys" edited by M. E. Fine and E. A. Starke ASTM STP 890 (American Society for Testing and Materials, Philadelphia, PA, 1986) p. 154.

Received 4 February 1994
and accepted 22 June 1995